ARTICLES

Journal of Semiconductors
(2023) 44, 032702
doi: 10.1088/1674-4926/44/3/032702

Exciton radiative lifetime in CdSe quantum dots

Zhimin Ji[1, 2] and Zhigang Song[1, †]

[1]State Key Laboratory of Superlattices and Microstructures, Institute of Semiconductors, Chinese Academy of Sciences, Beijing 100083, China
[2]Center of Materials Science and Optoelectronics Engineering, University of Chinese Academy of Sciences, Beijing 100049, China

Abstract: Colloidal CdSe quantum dots (QDs) are promising materials for solar cells because of their simple preparation process and compatibility with flexible substrates. The QD radiative recombination lifetime has attracted enormous attention as it affects the probability of photogenerated charges leaving the QDs and being collected at the battery electrodes. However, the scaling law for the exciton radiative lifetime in CdSe QDs is still a puzzle. This article presents a novel explanation that reconciles this controversy. Our calculations agree with the experimental measurements of all three divergent trends in a broadened energy window. Further, we proved that the exciton radiative lifetime is a consequence of the thermal average of decays for all thermally accessible exciton states. Each of the contradictory size-dependent patterns reflects this trend in a specific size range. As the optical band gap increases, the radiative lifetime decreases in larger QDs, increases in smaller QDs, and is weakly dependent on size in the intermediate energy region. This study addresses the inconsistencies in the scaling law of the exciton lifetime and gives a unified interpretation over a widened framework. Moreover, it provides valuable guidance for carrier separation in the thin film solar cell of CdSe QDs.

Key words: solar cells; CdSe quantum dot; radiative lifetime; scaling law; optical band gap; exciton fine structure; room temperature

Citation: Z M Ji and Z G Song, Exciton radiative lifetime in CdSe quantum dots[J]. *J. Semicond.*, 2023, 44(3), 032702. https://doi.org/10.1088/1674-4926/44/3/032702

1. Introduction

Owing to their size-tuneable optical properties[1] and high photoluminescence (PL) quantum yields at room temperature[2], colloidal semiconductor nanocrystals, also known as quantum dots (QDs), have been widely used in solar cells[3], lasers[4], light-emitting diodes[5], and bio/medical labelling[6]. CdSe QDs are studied as prototypes[7–12] because of their mature synthesis methods[7] and tuneable emission wavelengths covering the entire visible region[9]. Of particular interest is the influence of the nanocrystal size (and hence emission energy) on the radiative recombination lifetime. For purely scientific reasons, the radiative lifetime is important for unravelling the PL mechanism[13]; from a practical perspective, it affects the probability that photo-induced charges in solar cells will leave the QDs and be collected at the battery electrode[14]. However, three conflicting lifetime–size scaling laws have been reported following different experiments, contributing to a long-standing puzzle[15–20].

Javier *et al.* were the first to conduct a systematic experimental study of the influence of the nanocrystal size on the radiative lifetime under ambient conditions using time-resolved PL spectroscopy[15]. They explained the biexponential PL decay as a combination of the decays of an intrinsic band-edge exciton and a photoinduced charged exciton. The deduced radiative lifetimes of the intrinsic band-edge excitons are linearly correlated with the nanocrystal volume, yet are up to hundreds of nanoseconds, much longer than the currently accepted standard (tens of nanoseconds)[16–33].

Subsequently, van Driel *et al.*[16] provided a more reasonable radiative lifetime scale. They fitted the kinetic curves of their high-quality CdSe QDs to single exponential curves and found that within the emission frequency range of approximately 15 000–18 000 cm^{-1}, the radiative decay rate increased supralinearly with the emission frequency. Moreover, de Mello Donega *et al.*[17] reported a numerically similar result, suggesting that the spontaneous emission rate increases linearly with the PL peak energy. These data are plotted in Fig. 1(a), with the first exciton transition energy as the independent variable.

Gong *et al.*[18] questioned this lifetime–size relationship by arguing that these previous studies overrated the PL quantum yield and misestimated the QD size. Instead, they concluded that the radiative lifetime increases as the particle size decreases. By conducting a meta-analysis of the available experimental studies[19, 23–25] and performing complementary many-body pseudopotential calculations, Califano *et al.*[21] also revealed a slow increase in the radiative lifetime with an increase in the excitonic gap, as illustrated in Fig. 1(c).

Leistikow *et al.*[20] presented a third perspective. By measuring the total decay rate under different local densities of states, they revealed that, in the energy range of 2.0–2.25 eV, the radiative decay rate firstly increases and then decreases with increasing emission energy within a modest overall variation. This result also quantitatively coincided with the experimental observations of single CdSe nanocrystals obtained by Brokmann *et al.*[26]. These data are presented in Fig. 1(b).

According to these studies, the widespread controversy does not seem to be attributable to the diversity of measure-

Correspondence to: Z G Song, songzhigang@semi.ac.cn
Received 18 SEPTEMBER 2022; Revised 21 OCTOBER 2022.

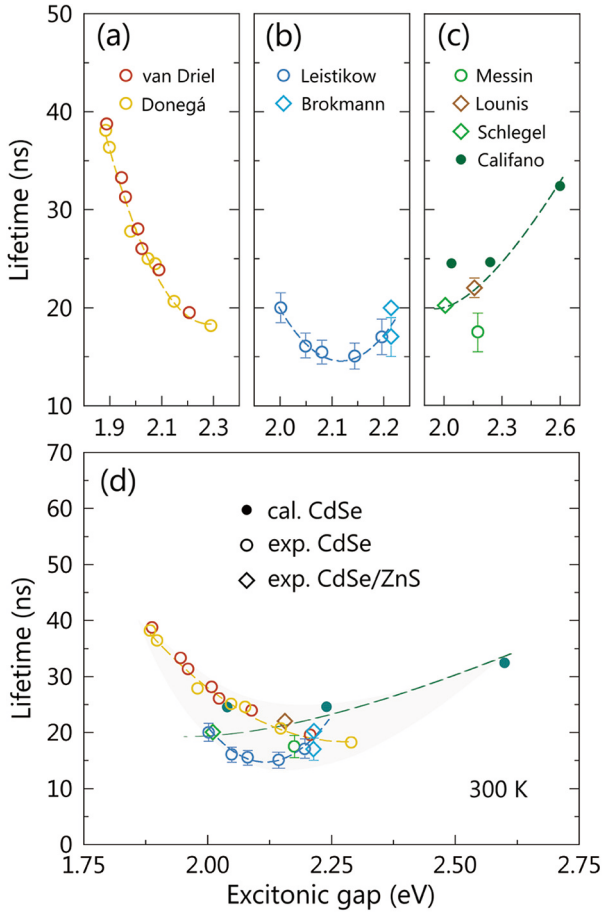

Fig. 1. (Color online) (a)–(c) Three trends in the relationship between the radiative lifetime and excitonic gap of CdSe QDs at room temperature. (d) Overall trend in a wider energy range. The small energy difference (millielectronvolt order) between the optical band gap and PL peak energy (electronvolt order) is ignored. Solid dots: calculated results obtained by Califano *et al.*[21]; circles: experimental values for CdSe QDs[16, 17, 20, 24]; hollow diamonds: experimental values for CdSe/ZnS core/shell QDs[23, 25, 26]; dashed curves: polynomial fitting curves; shaded region: permitted deviation.

ments (e.g., different sizing[17, 34–36] or lifetime[37] techniques) or the inhomogeneities of samples[12, 17, 18, 38]. This observation inevitably leads to considerations: (i) some typical studies are based on single nanocrystal fluorescence spectroscopy[23–26] and/or photon correlation techniques (which directly determine the radiative lifetime of a single exciton)[24, 25, 39]; (ii) most samples, especially well-passivated ZnS-coated QDs, manifest high luminescence efficiency[16, 17, 26]; and (iii) the emission energy or frequency, rather than physical size, is used as the independent variable in numerous studies[16, 17, 20]. Therefore, we attempted to identify the underlying causes of this dispute. Specifically, a critical factor that has been generally overlooked attracted our attention; i.e., the band-edge exciton energy coverage may vary in different experiments. We replotted Figs. 1(a)–1(c) in one coordinate system, as shown in Fig. 1(d). We found that, within the allowed error range, as the excitonic gap increases, the general trend of the radiative lifetime is an initial decrease followed by an increase, with subtle variations in the intermediate region of 2.1–2.3 eV. Accordingly, the long-running debate can be reconciled: different trends are derived from different band gap energy ranges.

For a more comprehensive understanding, we calculated the room-temperature exciton lifetime of CdSe QDs over a wide size range using the atomistic many-body pseudopotential approach[21, 22, 40, 41]. Our results are in excellent agreement with most published experimental values[16, 17, 20, 23–29]. In the wide energy window for the QD optical gap, we can identify all three previously reported conventional scaling laws. We show that the exciton radiative lifetime results from the thermal average of decays for all thermally accessible exciton states. Each of the three seemingly inconsistent scaling laws represents the trend in a specific size range; as the optical gap increases, the radiative lifetime decreases in large QDs and increases in small QDs, while exhibiting minor variations for intermediate-sized QDs. Our study effectively reconciles the previous standpoints and draws a unified conclusion.

2. Methods

The CdSe QDs were modelled in the three most common shapes of nanocrystals: spherical[17], prolate ellipsoidal[42, 43] and oblate ellipsoidal[44]. All ellipsoidal models were axially symmetric. For the prolate QDs, we subjectively chose an aspect ratio (ratio of the length of the longitudinal axis a to that of the transverse axis b) of 1.15 : 1. This value is equal to that observed by Moreels *et al.*[43] and is consistent with the previous experimental results of Murray *et al.*[8] of 1.0–1.3. Correspondingly, the aspect ratio of the oblate QDs was set to 1 : 1.15, which is also close to that reported by Chamarro *et al.*[44]. In the following, the effective diameter D is defined as the diameter of a sphere with the same volume as the ellipsoid $(D/2)^3 = b^2a$[44, 45].

Although most reported CdSe QDs have a wurtzite (WZ) crystal structure[2, 8–10], we instead considered the zinc blende (ZB) structure in this study to facilitate the comparison of the exciton fine structures under different hole-level splittings (*vide infra*)[33, 43–46]. The dot surfaces were fully passivated via ligand potentials to remove the localised surface states associated with dangling bonds away from the band gap[41, 47]. At low excitation density, the radiative lifetime is mainly determined by the spontaneous emission decay of single neutral excitons (e–h pairs)[16, 22]. Hence, we used the monoexciton radiative decay time as the QD radiative lifetime in our calculations.

The single-particle energies $\varepsilon_{e,h}$ and wave functions $\psi_{e,h}$ were obtained by solving the atomic empirical pseudopotential Schrödinger equations via the folded spectrum method[48, 49]:

$$(\hat{H} - \varepsilon_{ref})^2 \psi_{e,h} = (\varepsilon_{e,h} - \varepsilon_{ref})^2 \psi_{e,h}, \quad (1)$$

where $\hat{H} = -\frac{\hbar^2}{2m}\nabla^2 + V(\boldsymbol{r})$ is the semiempirical nonlocal pseudopotential Hamiltonian (including spin-orbit coupling) and $\sigma = \uparrow, \downarrow$ is the spin variable[40, 41]. By placing the reference energy ε_{ref} in the physically interesting range, one can calculate the energy states close to it, removing the need for orthogonalisation[48, 49].

The many-body excitonic energies E_γ and wave functions $\Psi^{(\gamma)}$ were obtained in the framework of the configuration interaction (CI) scheme[40, 41]:

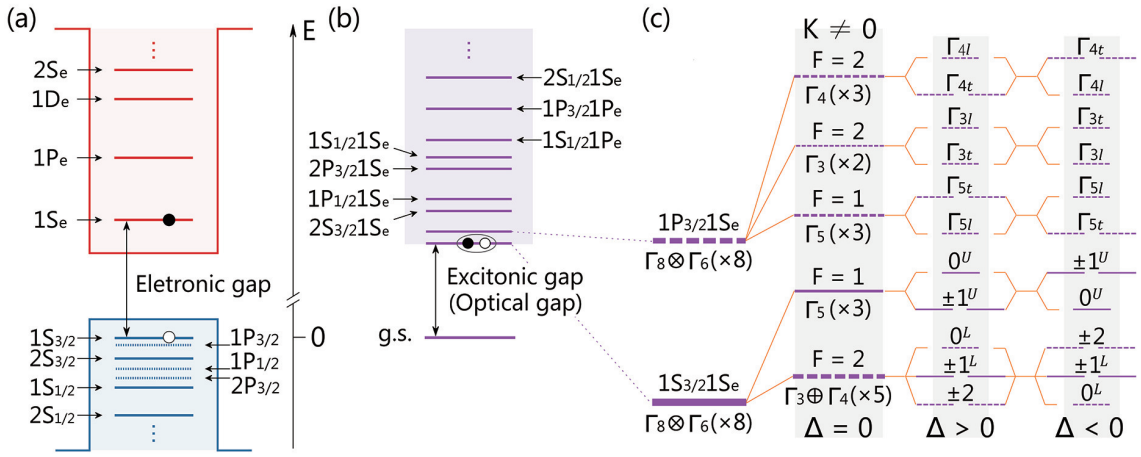

Fig. 2. (Color online) (a) Schematic of the near-edge single-particle levels of ZB-CdSe QD. The *P* hole states are indicated by short-dashed lines. (b) Scheme of band-edge exciton levels. (c) Diagram showing the exciton fine structures of $1S_{3/2}1S_e$ and $1P_{3/2}1S_e$ states. The dotted lines represent the 'dark' states, whereas the solid lines represent the 'bright' states. The numbers in brackets represent the degeneracy of energy levels. The total angular momentum of an exciton (F) is the sum of the total angular momentum of the hole (J_h) and electron (S_e). From left to right are the exciton states that exclude the exchange interaction ($K = 0$), include the exchange interaction ($K \neq 0$), and consider the anisotropic effect ($\Delta > 0$ and $\Delta < 0$).

$$\Psi^{(\gamma)} = \sum_{h=1}^{N_h}\sum_{e=1}^{N_e} C_{h,e}^{(\gamma)}\Phi_{h,e} \ , \tag{2}$$

$$\sum_{h'=1}^{N_h}\sum_{e'=1}^{N_e} \hat{H}_{he,\,h'e'}\, C_{h',e'}^{(\gamma)} = E_\gamma C_{h,e}^{(\gamma)} \ , \tag{3}$$

where N_e and N_h are the total number of single-particle electron and hole states included in the expansion of the exciton wave functions, respectively. The single-substitution Slater determinants $\{\Phi_{h,e}\}$ are constructed from the single-particle electron (ψ_e) and hole (ψ_h) wave functions. The coefficients $C_{h,e}^{(\gamma)}$ are the eigenstates of the CI Hamiltonian $\hat{H}_{he,\,h'e'}$ in the basis set $\{\Phi_{h,e}\}$. The excitonic gap E_0, also known as the optical band gap[50], is defined as the energy of the lowest excited state.

In the time-dependent perturbation theory framework, the radiative decay time τ_γ for the transition from $\Psi^{(\gamma)}$ to the ground state can be computed as[21, 22, 51]

$$\frac{1}{\tau_\gamma} = \frac{4nF_{loc}^2\alpha\omega_\gamma^3}{3c^2}\left|\boldsymbol{M}^{(\gamma)}\right|^2 \ , \tag{4}$$

where n is the refractive index of the surrounding medium (we took $n = 1.496$, the refractive index of toluene, the most common solvent for dissolving CdSe nanocrystals); α is the fine structure constant; c is the speed of light in a vacuum; ω_γ is the frequency of the emitted light; $F_{loc} = 3n^2/(2n^2 + \varepsilon_{QD})$ is the local-field correction factor based on the 'nanocrystal'-cavity model, which takes into account both the dielectric constants of the medium and the semiconductor, and ε_{QD} represents the high-frequency dielectric constant of the QD calculated using a modified Penn model[21, 22, 51, 52]; and $\boldsymbol{M}^{(\gamma)}$ is the dipole matrix element that can be established after obtaining the exciton eigenstates $C_{h,e}^{(\gamma)}$ by directly diagonalising the CI Hamiltonian[40]:

$$\boldsymbol{M}^{(\gamma)} = \sum_{h,e} C_{h,e}^{(\gamma)}\langle\psi_h|\hat{\boldsymbol{r}}|\psi_e\rangle \ . \tag{5}$$

The radiative lifetime $\tau_R(T)$ at temperature T (this text adopted room temperature $T = 300$ K) was calculated through Boltzmann statistics, as follows[21, 51]:

$$\frac{1}{\tau_R(T)} = \frac{\sum_\gamma \frac{1}{\tau_\gamma} e^{-(E_\gamma - E_0)/k_BT}}{\sum_\gamma e^{-(E_\gamma - E_0)/k_BT}} \ , \tag{6}$$

where k_B is the Boltzmann constant.

3. Results and discussion

3.1. Exciton fine structure

The optical properties of semiconductors depend principally on their electronic structures. In semiconductor nanocrystals smaller than the diameter of the bulk Bohr exciton, the electrons and holes are highly confined, and their energies exhibit discrete levels analogous to those of atoms (Ref. [1] and Fig. 2(a)). This condition is fulfilled for colloidal CdSe QDs with conventional sizes of 1.5–10 nm, as the exciton Bohr radius a_B of bulk CdSe is 5.6 nm[9]. Thus, the QD quantum states can be described using the notations employed to name the quantum states of atomic systems[53]. Moreover, at the atomic level, nanocrystals are structurally identical to their bulk counterpart; spherical CdSe QDs with a cubic (zinc blende) lattice structure preserve the T_d symmetry in the underlying bulk[40]. The lowest electronic state $1S_e$ is doubly degenerate with respect to its spin projection $s_z = \pm 1/2$[45], mainly transformed from the conduction band bottom of bulk CdSe according to the irreducible representation Γ_6 (in double group notation[54]) of the point group T_d[40]. Similarly, the highest hole state $1S_{3/2}$ is quadruple degenerate regarding projections $M = \pm 1/2, \pm 3/2$ of its total angular momentum $J_h = 3/2$[53, 55], mostly transformed from the valence band maximum of the bulk material according to the irreducible representation Γ_8 (Ref. [40] and Fig. 2(a)).

The energy-lowering Coulomb attraction binds the band-edge electron and hole together, giving rise to an exciton

state $1S_{3/2}1S_e$ ($\Gamma_8 \otimes \Gamma_6 = \Gamma_3 \oplus \Gamma_4 \oplus \Gamma_5$ in the language of group theory[54, 56]) with eight-fold degeneracy (Ref. [53] and Fig. 2(b)). Such degeneracy is lifted by the electron–hole exchange interaction K, which typically has a short-range and a long-range component, resulting in an 'exciton fine structure'[33, 40, 57]. The optically active ('bright') three-fold Γ_5 state with a total angular momentum of $F = 1$ has a higher exchange energy ΔE_X than the optically passive ('dark') degenerate three-fold Γ_4 and two-fold Γ_3 states with $F = 2$[33, 56]. This two-level exciton structure is shown schematically in the left column of Fig. 2(c).

The T_d symmetry can be broken by the intrinsic asymmetry of the hexagonal crystal field (in the wurtzite structure) and the non-spherical shape of QDs. These nanocrystal anisotropies split the hole state $1S_{3/2}$ into the 'heavy' ($M = \pm 3/2$) and 'light' ($M = \pm 1/2$) hole sublevels, further removing the degeneracy of exciton states[33, 46]. Labelling the exciton fine levels in terms of the projection M_F of their total angular momentum F[55], the high-lying Γ_5 state evolves into one level with $M_F = 0$ (marked by 0^U) and another with $M_F = \pm 1$ ($\pm 1^U$), whereas the low-lying $\Gamma_{3,4}$ states split into one level with $M_F = \pm 2$ (± 2), one with $M_F = \pm 1$ ($\pm 1^L$), and one with $M_F = 0$ (0^L). Here U and L correspond to the 'upper' and 'lower' states, respectively. States $\pm 1^L$, $\pm 1^U$, and 0^U are optically active, whereas states ± 2 and 0^L are optically passive. The net value Δ of the light–heavy hole level splitting determines which of the above states is the exciton ground state; i.e., the lowest energy exciton state is ± 2 for $\Delta > 0$ and 0^L for $\Delta < 0$. The net splitting $\Delta = \Delta_{in} + \Delta_{sh}$ is the sum of a crystal field component Δ_{in} and a non-spherical component Δ_{sh}. In the case of ZB-CdSe QDs, $\Delta_{in} = 0$; $\Delta_{sh} > 0$ for oblate crystals and $\Delta_{sh} < 0$ for prolate crystals. In the case of WZ-CdSe QDs, the growth axis coincides with the wurtzite c-axis, $\Delta_{in} > 0$; for oblate and spherical crystals, the order of exciton levels is the same as that in oblate ZB-CdSe QDs; for elongated crystals, Δ_{in} and Δ_{sh} are opposite in sign and mutual restraint, and the order of fine states may be one of the three cases when $K \neq 0$ in Fig. 2(c)[33, 46]. Note that the dependence of the spacing and order of these levels on the dimension, shape, and crystal structure has been debated extensively[33, 58–60]. As the main purpose of this article is to elucidate the size scaling law of radiative lifetime in spheroid CdSe QDs, we simulated only a specific class of systems in each Δ case. ZB-CdSe QDs are clearly the more convenient candidates. By designing the size and aspect ratio of ZB-CdSe QDs, one can simulate the band-edge exciton fine structure of WZ-CdSe QDs[46]. In fact, in the strong confinement regime, the hexagonal crystal field effect is easily offset or masked by the deviations from sphericity. Specifically, the small prolate WZ- and ZB-CdSe QDs with an aspect ratio of 1.15 : 1 have similar exciton fine structures and are optically indistinguishable on the nanosecond time scale[43].

It has long been known that in CdSe QDs, the hole state $1P_{3/2}$ is energetically the closest to the hole state $1S_{3/2}$ (Ref. [53] and Fig. 2(a)). Accordingly, in the two-particle picture Fig. 2(b), the energy level for the $1P_{3/2}1S_e$ exciton is close to that for the $1S_{3/2}1S_e$ exciton. Therefore $1P_{3/2}1S_e$ may play a role in the optical transition process[18, 33], and a related discussion is necessary. Similar to the hole state $1S_{3/2}$, in the T_d point group, the hole state $1P_{3/2}$ also originates from the Γ_8 bulk valence bands[40]. Considering that the electron state $1S_e$ has Γ_6 symmetry, the direct product $\Gamma_8 \otimes \Gamma_6$ leads to three irreducible T_d representations $\Gamma_3 \oplus \Gamma_4 \oplus \Gamma_5$. As pointed out by Ajiki *et al.*[61] and Sercel *et al.*[33], the long-range exchange interaction for the eight-fold states $1P_{3/2}1S_e$ shifts the five-fold $F = 2$ (Γ_3 and Γ_4) level above the three-fold $F = 1$ (Γ_5) level. Our atomic calculations show that the $\Gamma_{3,4}$ states in $1P_{3/2}1S_e$ are pre-split for spherical ZB-CdSe QDs, contrary to the $1S_{3/2}1S_e$ exciton manifold, where the Γ_4 states are unsplit from the Γ_3 states. Furthermore, the sublevels of exciton $1P_{3/2}1S_e$ are more densely packed than those of $1S_{3/2}1S_e$[33]. Consequently, additional split fine levels due to anisotropic effects can easily cross or overlap with each other. Continuing to use the total angular momentum projection to denote the fine energy levels would cause confusion, because it is difficult to clearly refer to 'upper' and 'lower'. Labelling the exciton fine levels with Koster's notation[54] is more convenient. As shown in Fig. 2(c), in the presence of nanocrystal asymmetries, the Γ_3 states split into a longitudinal exciton Γ_{3l} and a transverse exciton Γ_{3t}, whereas the Γ_4 and Γ_5 states each split into a longitudinal singlet (Γ_{4l}, Γ_{5l}) and a transverse doublet (Γ_{4t}, Γ_{5t})[56]. It is noteworthy that the exciton fine structure depends strongly on the size and shape of the QD, the actual order of the $1P_{3/2}1S_e$ sublevels may not exactly coincide with those depicted in the figure. Although the exciton states $1P_{3/2}1S_e$ are dipole prohibited due to parity[33, 53], these states are not completely zero, because of the atomic characteristics of single-particle wavefunctions and the interactions between exciton configurations[22].

3.2. Optical band gap sizing curve

The excitonic gap is often regarded as a substitute measurement for the QD size because of their one-to-one correspondence[17]. Considering that the band gap can be directly observed in optical measurements of the exciton radiative lifetime[37] and that excitonic gap measurements are more accurate and repeatable than QD size measurements[17], it is more suitable to use a scaling law for the radiative lifetime as a function of the optical band gap, as shown in Fig. 1.

Correct estimation of the optical band gap is a prerequisite for the energy-dependent reliability. As a function of the QD effective diameter (in nanometers), our calculation of the excitonic gap (in electronvolts) of ZB-CdSe QDs is compared with the available experimental data[62–68], as shown in Fig. 3. Notably, within the size range considered in this study, most calculated values and experimental data fall on the empirical curve proposed by Čapek *et al.*[63]:

$$E_g^{QD}(D) = 1.74 + \frac{1}{0.22D^2 - 0.36D + 0.89}. \quad (7)$$

This fitting method is derived from the tight-binding calculation of PbSe nanocrystals by Allan *et al.*[69]:

$$E_g^{QD}(D) = E_g(\infty) + \frac{1}{\zeta_1 D^2 - \zeta_2 D + \zeta_3}, \quad (8)$$

where ζ_1, ζ_2, and ζ_3 are fitting parameters. This calculation focuses on the size range corresponding to strongly constrained systems ($D \leqslant 2a_B$, a_B is 46 nm for bulk PbSe[69] and 5.6 nm for bulk CdSe[50]). For comparison, under strong confinement conditions, the first exciton transition energy of a spherical QD of diameter D, calculated using the effective

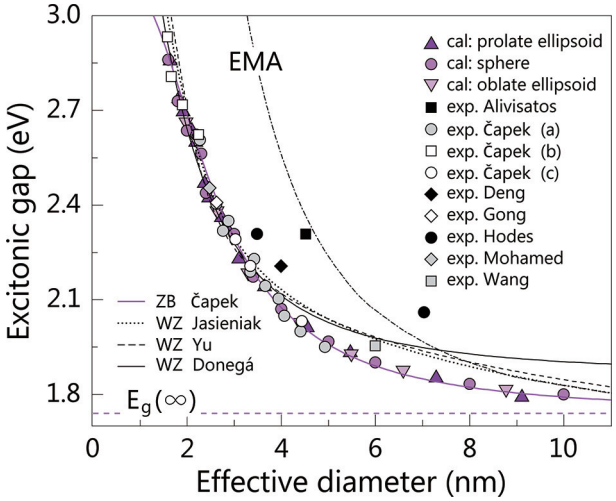

Fig. 3. (Color online) Excitonic gap of ZB-CdSe QDs as a function of the effective diameter. The current calculation results are represented by purple points, where the regular triangles, dots, and inverted triangles denote the data for prolate, spherical, and oblate QDs, respectively. Experimental data: ■ from Ref. [67]; ●, □, and ○ from Ref. [63]; ◆ from Ref. [65]; ◇ from Ref. [62]; ● from Ref. [68]; ◆ from Ref. [66]; ■ from Ref. [64]. An empirical fitting curve for ZB-CdSe QDs by Čapek *et al.*[63], (purple solid curve) and WZ-CdSe sizing curves according to Jasieniak *et al.*[71] (black dotted curve), Yu *et al.*[35] (black dashed curve), and de Mello Donega *et al.*[17] (black solid curve) are displayed. Dash–dot curve: prediction of EMA by Brus *et al.*[42]; purple dashed line: band gap of bulk CdSe at room temperature[50].

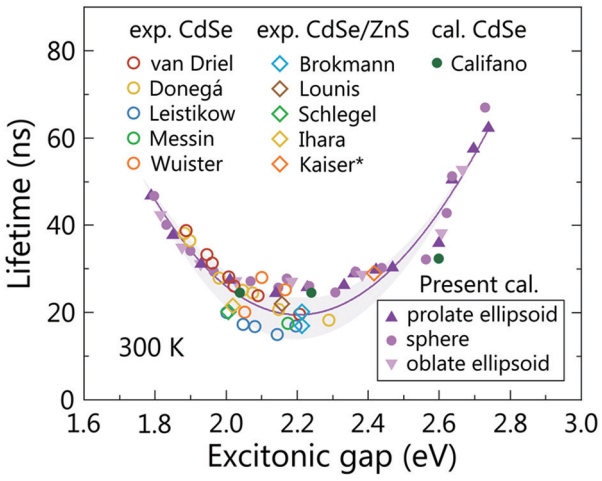

Fig. 4. (Color online) Comparison of our simulated QD radiative lifetimes with experimental data over a wide energy window. Purple solid points: present calculated values, where the regular triangles, dots, and inverted triangles represent the data for prolate, spherical, and oblate QDs, respectively. Green solid dots: calculated results by Califano *et al.*[21]; circles: experimental values for CdSe QDs[16, 17, 20, 24, 27]; diamonds: experimental values for CdSe/ZnS core/shell QDs[23,25, 26, 28, 29]; purple curve: polynomial fitting curve; shaded region: permitted deviation. Note: * All experiments were conducted in a medium with n = 1.496, except for Kasier's measurement in water[28].

mass approximation (EMA), is as follows[8, 42] (dash–dot curve in Fig. 3):

$$E_g^{QD}(D) = E_g(\infty) + \frac{2\pi^2\hbar^2}{D^2}\left[\frac{1}{m_e^*} + \frac{1}{m_h^*}\right] - \frac{1.8e^2}{\varepsilon_\infty D/2}. \quad (9)$$

In the large-size limit, this approximation agrees reasonably well with the ZB-CdSe empirical curve; however, it overestimates the results for smaller nanocrystals. The unjustified assumption of the infinite potential barrier at the surface and the over-approximation of the parabolic shape of energy bands at even higher wave vectors are primarily responsible for the deviation[43, 70].

By contrast, the fitting curves by de Mello Doneg *et al.*[17], Yu *et al.*[35], and Jasieniak *et al.*[71] for WZ-CdSe QDs closely approximate the empirical curve for ZB-CdSe QDs for dot sizes smaller than 3.8 nm. However, divergences are gradually notable for diameters greater than 4 nm because of the interior bonding geometry of the lattice structures[43, 60]. These curves are graphically indistinguishable in the high-energy region, as the crystal field effect found exclusively in the wurtzite structure is negligible compared to the limit of strong confinement[60]. The differences in the sizing curves further support the appropriateness of describing the quantum confinement effect in terms of energy dependence rather than size dependence.

3.3. Size dependence of the exciton radiative lifetime at room temperature

Based on the established 'particle size–optical gap' relationship, we compared the room-temperature radiative lifetime (in nanoseconds) of CdSe QDs predicted by our method with the experimental results from previous study. It is worth notifying that we deliberately chose the results for single QDs or diluted solutions of QDs with narrow particle size distribution when collecting experimental data. As shown in Fig. 4, our theoretical values agree well with most experimental results[16, 17, 20, 23–29]. The complexity of the dielectric environment[20] and the presence of nonradiative recombination channel[18] may be the major factors in the deviation of our results from the experiments. In addition, the lack of experimental data in high-energy regions is due to the inability to detect PL signals effectively at room temperature. This section illustrates how the exciton fine structure of the QDs determines the non-monotonic variation.

As described in Section 3.2, although CdSe QDs of different shapes may have different exciton fine structures, all the lowest exciton states are optically passive, followed by higher-lying optically active states[17, 60]. Accordingly, a three-level thermal equilibrium model can be extracted, which includes a ground-state level, lower (dark) energy level, and higher (bright) energy level.

de Mello Donega *et al.*[17] argued that only the higher bright level should be considered because of the inappreciable contribution of the dark states to light emission. However, as the exciton population follows the Boltzmann distribution[21, 51], the bright excitonic level of energy E_γ is not completely thermally occupied, but rather has an excitation probability $p_\gamma = e^{-(E_\gamma - E_0)/k_B T}$ relative to the lowest dark level. The dark level, playing the role of a storage tank of the exciton population[18, 72], could prolong the measured apparent radiative lifetime several times. Thus, it should not be ignored.

Notably, van Driel *et al.*[16] reported a similar result based on an exciton fine structure model. They held that the radiative recombination rate is determined by the thermal occupa-

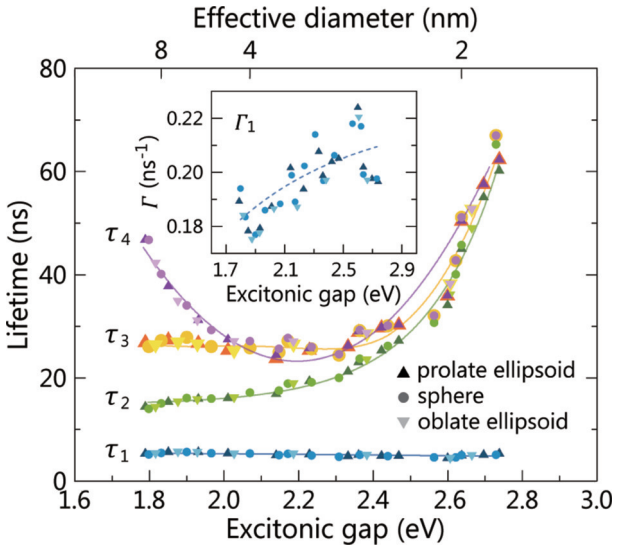

Fig. 5. (Color online) Dependence of the room-temperature radiative lifetime on the optical gap for different levels of complexity in the many-particle treatment. For the meanings of the regular triangles, dots, and inverted triangles, see Fig. 4. τ_1 (blue points): only the bright states in the $1S_{3/2}1S_e$ exciton manifold; τ_2 (green points): thermal average of the $1S_{3/2}1S_e$ exciton manifold; τ_3 (orange points): thermal average of exciton states derived from $1S_{3/2}1S_e$ and $1P_{3/2}1S_e$; τ_4 (purple points): thermal average of all thermally accessible states (same data as denoted by the purple data points in Fig. 4). On the upper *x*-axis, three representative QD effective sizes are shown. Inset: dependence of the radiative rate of the $1S_{3/2}1S_e$-derived bright exciton on the excitonic gap.

tion of a dark exciton state, whose position is higher than that of a bright state. This model contradicts the confirmed experimental facts[45, 73] leading to their complementary tight-binding calculated decay rates being approximately 75% smaller than the experimental observations.

The 'dark–bright' exciton fine structure model we discussed in the preceding section was proposed by Efros *et al.* and was strongly supported by measurements of the time decay of dark excitons in CdSe nanocrystals under low-temperature external magnetic fields[45]. Nevertheless, Gong *et al.*[18] noted that the model is inaccurate in the high-temperature limit (including at room temperature), as the higher-energy $1P_{3/2}1S_e$ exciton manifold is also thermally accessible. Furthermore, Califano *et al.*[21, 22] found that the contributions of higher exciton states should be included when calculating the room-temperature thermal average of the radiative rate.

To address these contraries, we calculated the room-temperature radiative lifetime at different levels of complexity corresponding to (i) τ_1: only the bright states in the $1S_{3/2}1S_e$ exciton manifold, (ii) τ_2: the thermal average of the $1S_{3/2}1S_e$ exciton manifold, (iii) τ_3: the thermal average of exciton states derived from $1S_{3/2}1S_e$ and $1P_{3/2}1S_e$, and (iv) τ_4: the thermal average of all thermally accessible states. Our results are organised in Fig. 5.

For spherical ZB-CdSe QDs, only the three-fold Γ_5 state ($F = 1$) is bright among the energy states associated with the optical $1S_{3/2}1S_e$ transitions. For the ellipsoid QDs, although state $\pm1^L$ is also optically allowed, its oscillator strength is 1–3 orders of magnitude smaller than that of the upper excitons $\pm1^U$ and 0^U evolved from the Γ_5 state. Therefore, we decided to address only these upper bright states in this paragraph, leaving the lowest bright state $\pm1^L$ for the next paragraph. In Fig. 5, at first glance, the bright exciton radiative lifetime τ_1 shows little size dependence. However, a sublinear relation is presented (inset) when the data are replotted as the radiative rate (in ns^{-1}) versus the excitonic gap. According to Eq. (4), the radiative rate $\Gamma_\gamma = \tau_\gamma^{-1}$ is the culmination of two opposite trends as the QD size is reduced: an increase in the exciton transition energy (due to the quantum confinement effect) and a decrease in the overlap between the electron and hole wave functions (leading to smaller dipole matrix elements $|M|^2$)[22]. On the basis of the relationship between the momentum and dipole matrix elements $\langle\psi_e|\hat{\boldsymbol{p}}|\psi_h\rangle = im\omega_{eh}\langle\psi_e|\hat{\boldsymbol{r}}|\psi_h\rangle$ and the assumption that $\langle\psi_e|\hat{\boldsymbol{p}}|\psi_h\rangle$ is independent of the nanocrystal size, one can predict $\Gamma_\gamma \propto \omega_\gamma$[16, 74]. For the same reason, de Mello Doneg *et al.* also presented a linear dependence of the bright exciton radiative rate on the emission frequency in the framework of the $\mathbf{k}\cdot\mathbf{p}$ theory[17]. This prediction is consistent with several earlier EMA studies[75, 76], which pointed out that the oscillator strength f of the band-edge excitons has a weak size dependence: $f_\gamma \propto \omega_\gamma^{-1}$. Considering that the emitted oscillator strength is related to the spontaneous emission rate $f_\gamma \propto \Gamma_\gamma\omega_\gamma^{-2}$[77], a linear relationship can be obtained: $\Gamma_\gamma = \text{const}\cdot\omega_\gamma$. Nonetheless, because of the atomistic character of single-particle wave functions, as well as the interstate coupling of exciton configurations[22], our calculations show that many-body dipole matrix elements increase with increasing nanocrystal diameter, resulting in a sublinear band gap-dependent radiative rate.

Although τ_1 decreases as the QD diameter decreases, the thermally averaged lifetime τ_2 of the exciton states derived from $1S_{3/2}1S_e$ increases (Fig. 5). As mentioned previously, the thermal excitation probability of a bright exciton level is inversely exponentially related to the energy separation between it and the lowest dark state: $p_\gamma = e^{-(E_\gamma - E_0)/k_BT}$. Within the $1S_{3/2}1S_e$ exciton manifold in spherically symmetric CdSe QDs, only the upper state ($F = 1$) is bright, and its distance from the ground dark state is described as exchange splitting ΔE_X. In general, ΔE_X consists of a short-range ($\Delta E_X^{(SR)}$) and a long-range ($\Delta E_X^{(LR)}$) component[33, 40, 57]. In the multiband EMA represented by Efros *et al.*[33, 45], $\Delta E_X^{(SR)}$ scales as D^{-3} with the nanocrystal diameter D, and $\Delta E_X^{(LR)}$ is approximately 2.5 times larger than $\Delta E_X^{(SR)}$ in CdSe. Atomistic pseudopotential calculations[40] showed instead the total exchange splitting $\Delta E_X \sim D^{-2}$, which was confirmed by later experiments[78]. For the slightly prolate and oblate ellipsoidal QDs, asymmetry effects can be considered a perturbation to the exchange interaction, especially when the dots are small. The distance between the lowest bright state $\pm1^L$ and the ground dark state varies less with the QD size, converging to $|3\Delta/4|$ at the smallest limit (Δ is the total value of the light–heavy hole level splitting)[33]. In contrast, the size-dependent behaviours of the energy distances from the upper bright states $\pm1^U$ and 0^U to the ground state are similar to that of the exchange splitting in spherical ZB-CdSe QDs. Ultimately, the moderate increase in the radiative decay rate of the bright excitons is insufficient to balance the drastic decline in the corresponding thermal population as the QD size is reduced. Hence, the latter should be responsible for increasing the weighted aver-

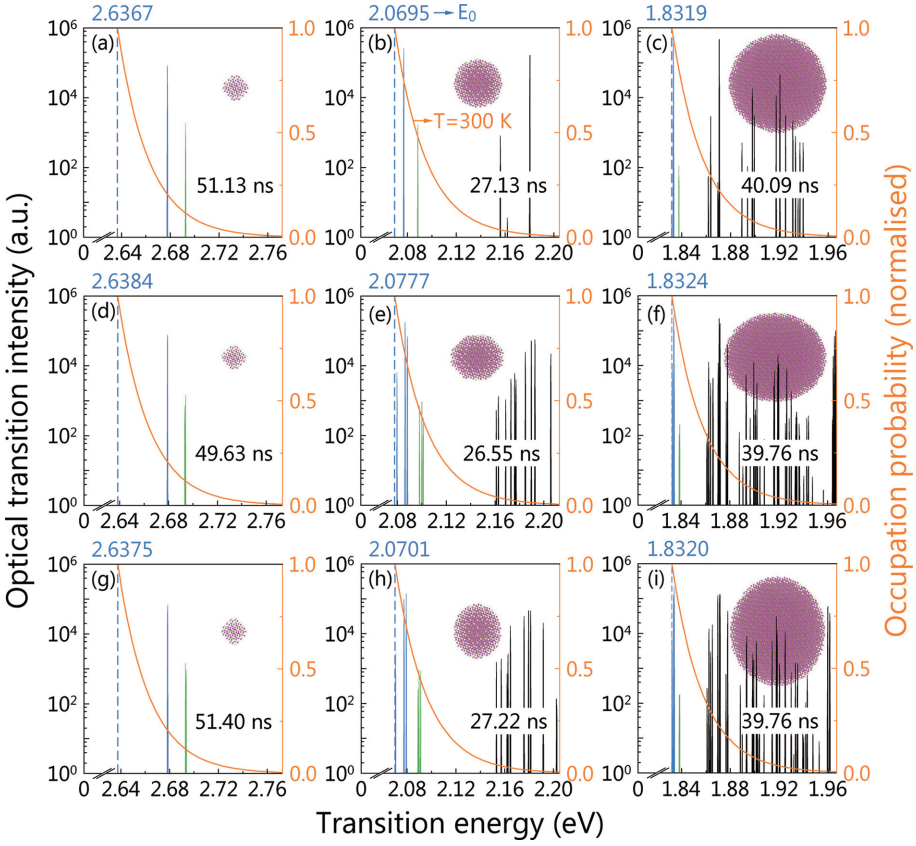

Fig. 6. (Color online) Single-exciton absorption spectra of (a–c) the spherical ZB-CdSe QDs with diameters of 2 (left), 4 (middle), and 8 nm (right) as well as those of (d–f) the oblate ZB-CdSe QDs and (g–i) prolate ZB-CdSe QDs with excitonic gaps similar to these spherical QDs. Blue dashed line: position of the first exciton transition energy; blue solid line: oscillator strength line of bright states in $1S_{3/2}1S_e$; green solid line: oscillator strength line of `bright' states in $1P_{3/2}1S_e$; black solid line: oscillator strength line of higher-energy states; orange curve: Boltzmann population at 300 K. The transition intensity is logarithmic (left), whereas the distribution probability is linear (right). The QD radiative lifetime at 300 K is also shown. Inset: 3D model of the QDs (to scale).

age lifetime τ_2 with the excitonic gap. These findings also confirm that the integrated extinction coefficients increase with increasing particle radius[18, 35, 71].

It is also noteworthy that some new features emerged when higher excitonic states were taken into account. For ordinary colloidal CdSe QDs, the exchange splitting is several to tens of millielectronvolts depending on the particle size, comparable to or even smaller than k_BT at 300 K (approximately 25.8 meV). In this case, the higher exciton states may also be thermally accessible. Gong *et al.* also stated that the $1P_{3/2}1S_e$ exciton should not be ignored[18]. Figs. 6(a)–6(c) depict the single-exciton absorption spectra of the spherical ZB-CdSe QDs with diameters of 2, 4, and 8 nm (corresponding to the three regions in Fig. 2) and the thermal population of these exciton states at room temperature. In the same way, Figs. 6(d)–6(f) and Figs. 6(g)–6(i) sketch the exciton states of the oblate and prolate QDs with excitonic gaps similar to these spherical QDs, respectively. It can be seen that in these nine nanocrystals, the $1P_{3/2}1S_e$ excitons are all thermally accessible. Exchange interaction and shape asymmetry split the eight-fold exciton state $1P_{3/2}1S_e$ into five partially degenerate dark states (of Γ_3 and Γ_4) and three partially degenerate 'bright' states (of Γ_5). Here, 'bright' appears inside quotation marks because although the Γ_5 symmetry is optically allowed, the parity difference of electrons and holes renders the Γ_5 states in $1P_{3/2}1S_e$ with oscillator strength several orders of magnitude smaller than that of the bright states in $1S_{3/2}1S_e$[53]. The participation of the optically inactive exciton manifold $1P_{3/2}1S_e$ could extend the calculated average lifetime τ_3. When the nanocrystal is small, the probability of $1P_{3/2}1S_e$ excitons being thermally occupied is very low, and their influence on the average lifetime is negligible. As the dot size increases, however, the extension to the total lifetime τ_3 becomes progressively more significant due to the increased involvement of $1P_{3/2}1S_e$. Moreover, τ_3 tends to be constant at the large size limit because when the nanocrystal is large enough, $1P_{3/2}1S_e$ will be close to the ground state, and its thermal population will almost saturate. This result is also consistent with the recent EMA calculations of Sercel *et al.*[33].

It is well known that higher-energy exciton states (including, but not limited to, $1P_{3/2}1S_e$) approach the ground state as the nanocrystal size increases[53]. Thus, the number of thermally accessible states increases substantially (Fig. 6), indicating more significant contributions to the average lifetime for larger Boltzmann populations. In addition, the lifetime dramatically increases owing to the dark states forming the majority. This increase overcompensates for the decrease caused by the $1S_{3/2}1S_e$ bright sublevels that are closer to the ground state under the larger size limit. All thermally accessible exciton states ultimately induce the profile of the QD radiative lifetime τ_4, as shown in Fig. 5. In the low energy region, the lifetime τ_4 decreases with the excitonic gap. However, it is worth noting that this conclusion does not support the assumption of de Mello Donega *et al.*, that is, the decays of

bright excitons alone lead to the linear increase in the QD spontaneous emission rate with emission energy. Our calculations show that the thermally averaged radiative lifetime is several times longer than the bright exciton lifetime.

4. Conclusion

We investigated the room-temperature radiative lifetime of CdSe QDs over a wide size range using a fully atomistic theory that accounts for many-body effects. Our theoretical values are in good agreement with most experimental data. We showed that the QD radiative lifetime is a consequence of the thermal average of all thermally accessible exciton states. The unified size scaling law described herein can be considered globally in a broader energy window, in contrast to the three contradictory local trends seen in their corresponding energy windows. Accordingly, the exciton lifetime in each emission frequency band can be predicted effectively. This study resolves a long-standing knowledge gap in the behaviour of CdSe QDs. Moreover, it provides valuable guidance for carrier separation in the colloidal QDs that make up the photovoltaic absorber material, opening the way for future enhancements and use of this technology.

Acknowledgements

Zhimin Ji is grateful to A.P. Yuan Qu and Pro. Jun-Wei Luo for valuable discussions. Zhigang Song was supported by the National Key Research and Development Program of China under Grant No. 2021YFB2800304. We would like to thank Editage (www.editage.cn) for English language editing.

References

[1] Efros A L, Rosen M. The electronic structure of semiconductor nanocrystals. Annu Rev Mater Sci, 2000, 30, 475
[2] Qu L H, Peng X G. Control of photoluminescence properties of CdSe nanocrystals in growth. J Am Chem Soc, 2002, 124, 2049
[3] Kirmani A R, Luther J M, Abolhasani M, et al. Colloidal quantum dot photovoltaics: Current progress and path to gigawatt scale enabled by smart manufacturing. ACS Energy Lett, 2020, 5, 3069
[4] Park Y S, Roh J, Diroll B T, et al. Colloidal quantum dot lasers. Nat Rev Mater, 2021, 6, 382
[5] Pradhan S, Dalmases M, Baspinar A, et al. Highly efficient, bright, and stable colloidal quantum dot short-wave infrared light-emitting diodes. Adv Funct Mater, 2020, 30, 2004445
[6] Kairdolf B A, Smith A M, Stokes T H, et al. Semiconductor quantum dots for bioimaging and biodiagnostic applications. Annu Rev Anal Chem, 2013, 6, 143
[7] Qu L H, Peng Z A, Peng X G. Alternative routes toward high quality CdSe nanocrystals. Nano Lett, 2001, 1, 333
[8] Murray C B, Norris D J, Bawendi M G. Synthesis and characterization of nearly monodisperse CdE (E = sulfur, selenium, tellurium) semiconductor nanocrystallites. J Am Chem Soc, 1993, 115, 8706
[9] Empedocles S, Bawendi M. Spectroscopy of single CdSe nanocrystallites. Acc Chem Res, 1999, 32, 389
[10] Underwood D F, Kippeny T, Rosenthal S J. Ultrafast carrier dynamics in CdSe nanocrystals determined by femtosecond fluorescence upconversion spectroscopy. J Phys Chem B, 2001, 105, 436
[11] Munro A M, Chandler C, Garling M, et al. Phenyldithiocarbamate ligands decompose during nanocrystal ligand exchange. J Phys Chem C, 2016, 120, 29455
[12] Labeau O, Tamarat P, Lounis B. Temperature dependence of the luminescence lifetime of single CdSe/ZnS quantum dots. Phys Rev Lett, 2003, 90, 257404
[13] Wang X Y, Qu L H, Zhang J Y, et al. Surface-related emission in highly luminescent CdSe quantum dots. Nano Lett, 2003, 3, 1103
[14] Leontiadou M A, Tyrrell E J, Smith C T, et al. Influence of elevated radiative lifetime on efficiency of CdSe/CdTe type II colloidal quantum dot based solar cells. Sol Energy Mater Sol Cells, 2017, 159, 657
[15] Javier A, Magana D, Jennings T, et al. Nanosecond exciton recombination dynamics in colloidal CdSe quantum dots under ambient conditions. Appl Phys Lett, 2003, 83, 1423
[16] van Driel A F, Allan G, Delerue C, et al. Frequency-dependent spontaneous emission rate from CdSe and CdTe nanocrystals: Influence of dark states. Phys Rev Lett, 2005, 95, 236804
[17] de Mello Donegá C, Koole R. Size dependence of the spontaneous emission rate and absorption cross section of CdSe and CdTe quantum dots. J Phys Chem C, 2009, 113, 6511
[18] Gong K, Zeng Y H, Kelley D F. Extinction coefficients, oscillator strengths, and radiative lifetimes of CdSe, CdTe, and CdTe/CdSe nanocrystals. J Phys Chem C, 2013, 117, 20268
[19] Crooker S A, Barrick T, Hollingsworth J A, et al. Multiple temperature regimes of radiative decay in CdSe nanocrystal quantum dots: Intrinsic limits to the dark-exciton lifetime. Appl Phys Lett, 2003, 82, 2793
[20] Leistikow M D, Johansen J, Kettelarij A J, et al. Size-dependent oscillator strength and quantum efficiency of CdSe quantum dots controlled via the local density of states. Phys Rev B, 2009, 79, 045301
[21] Califano M, Franceschetti A, Zunger A. Temperature dependence of excitonic radiative decay in CdSe quantum dots: The role of surface hole traps. Nano Lett, 2005, 5, 2360
[22] Califano M, Franceschetti A, Zunger A. Lifetime and polarization of the radiative decay of excitons, biexcitons, and trions in CdSe nanocrystal quantum dots. Phys Rev B, 2007, 75, 115401
[23] Schlegel G, Bohnenberger J, Potapova I, et al. Fluorescence decay time of single semiconductor nanocrystals. Phys Rev Lett, 2002, 88, 137401
[24] Messin G, Hermier J P, Giacobino E, et al. Bunching and antibunching in the fluorescence of semiconductor nanocrystals. Opt Lett, 2001, 26, 1891
[25] Lounis B, Bechtel H A, Gerion D, et al. Photon antibunching in single CdSe/ZnS quantum dot fluorescence. Chem Phys Lett, 2000, 329, 399
[26] Brokmann X, Coolen L, Dahan M, et al. Measurement of the radiative and nonradiative decay rates of single CdSe nanocrystals through a controlled modification of their spontaneous emission. Phys Rev Lett, 2004, 93, 107403
[27] Wuister S F, de Mello Donegá C, Meijerink A. Local-field effects on the spontaneous emission rate of CdTe and CdSe quantum dots in dielectric media. J Chem Phys, 2004, 121, 4310
[28] Kaiser U, Jimenez de Aberasturi D, Malinowski R, et al. Multiplexed measurements by time resolved spectroscopy using colloidal CdSe/ZnS quantum dots. Appl Phys Lett, 2014, 104, 041901
[29] Ihara T, Kanemitsu Y. Spectral diffusion of neutral and charged exciton transitions in single CdSe/ZnS nanocrystals due to quantum-confined Stark effect. Phys Rev B, 2014, 90, 195302
[30] Wu X W, Gong M, Dong C H, et al. Anti-bunching and luminescence blinking suppression from plasmon-interacted single CdSe/ZnS quantum dot. Opt Express, 2010, 18, 6340
[31] Masuo S, Naiki H, Machida S, et al. Photon statistics in enhanced fluorescence from a single CdSe/ZnS quantum dot in the vicinity of silver nanoparticles. Appl Phys Lett, 2009, 95, 193106
[32] Yuan C T, Yu P, Ko H C, et al. Antibunching single-photon emission and blinking suppression of CdSe/ZnS quantum dots. ACS Nano, 2009, 3, 3051
[33] Sercel P C, Efros A L. Band-edge exciton in CdSe and other II-VI and III-V compound semiconductor nanocrystals - revisited. Nano

Lett, 2018, 18, 4061
[34] Maes J, Castro N, de Nolf K, et al. Size and concentration determination of colloidal nanocrystals by small-angle X-ray scattering. Chem Mater, 2018, 30, 3952
[35] Yu W W, Qu L H, Guo W Z, et al. Experimental determination of the extinction coefficient of CdTe, CdSe, and CdS nanocrystals. Chem Mater, 2003, 15, 2854
[36] Ebenstein Y, Mokari T, Banin U. Fluorescence quantum yield of CdSe/ZnS nanocrystals investigated by correlated atomic-force and single-particle fluorescence microscopy. Appl Phys Lett, 2002, 80, 4033
[37] Demas J. Excited state lifetime measurements. New York: Academic Press, 1983
[38] Kuçur E, Boldt F M, Cavaliere-Jaricot S, et al. Quantitative analysis of cadmium selenide nanocrystal concentration by comparative techniques. Anal Chem, 2007, 79, 8987
[39] Michler P, Imamoğlu A, Mason M D, et al. Quantum correlation among photons from a single quantum dot at room temperature. Nature, 2000, 406, 968
[40] Franceschetti A, Fu H, Wang L W, et al. Many-body pseudopotential theory of excitons in InP and CdSe quantum dots. Phys Rev B, 1999, 60, 1819
[41] Luo J W, Stradins P, Zunger A. Matrix-embedded silicon quantum dots for photovoltaic applications: A theoretical study of critical factors. Energy Environ Sci, 2011, 4, 2546
[42] Brus L E. Electron–electron and electron–hole interactions in small semiconductor crystallites: The size dependence of the lowest excited electronic state. J Chem Phys, 1984, 80, 4403
[43] Moreels I, Rainò G, Gomes R, et al. Band-edge exciton fine structure of small, nearly spherical colloidal CdSe/ZnS quantum dots. ACS Nano, 2011, 5, 8033
[44] Chamarro M, Dib M, Gourdon C, et al. Electronic structure of O-D exciton ground state in CdSe nanocrystals. MRS Online Proc Libr, 1996, 452, 341
[45] Efros A L, Rosen M, Kuno M, et al. Band-edge exciton in quantum dots of semiconductors with a degenerate valence band: Dark and bright exciton states. Phys Rev B, 1996, 54, 4843
[46] Rodina A V, Efros A L. Radiative recombination from dark excitons in nanocrystals: Activation mechanisms and polarization properties. Phys Rev B, 2016, 93, 155427
[47] Wang L W, Zunger A. Pseudopotential calculations of nanoscale CdSe quantum dots. Phys Rev B, 1996, 53, 9579
[48] Wang L W, Zunger A. Electronic structure pseudopotential calculations of large (.apprx.1000 atoms) Si quantum dots. J Phys Chem, 1994, 98, 2158
[49] Wang L W, Zunger A. Solving Schrödinger's equation around a desired energy: Application to silicon quantum dots. J Chem Phys, 1994, 100, 2394
[50] Meulenberg R W, Lee J R I, Wolcott A, et al. Determination of the exciton binding energy in CdSe quantum dots. ACS Nano, 2009, 3, 325
[51] An J M, Franceschetti A, Zunger A. The excitonic exchange splitting and radiative lifetime in PbSe quantum dots. Nano Lett, 2007, 7, 2129
[52] Senden T, Rabouw F T, Meijerink A. Photonic effects on the radiative decay rate and luminescence quantum yield of doped nanocrystals. ACS Nano, 2015, 9, 1801
[53] Ekimov A I, Hache F, Schanne-Klein M C, et al. Absorption and intensity dependent photoluminescence measurements on CdSe quantum dots: Assignment of the first electronic transitions. J Opt Soc Am B, 1993, 10, 100
[54] Dresselhaus M, Dresselhaus G, Jorio A. Group theory: Application to the physics of condensed matter. Berlin, Heidelberg: Springer, 2007, 10
[55] In spherical approximation, the electron (hole) state is characterised by the total angular momentum $\mathbf{J} = \mathbf{s} + \mathbf{l} + \mathbf{j}$, where $\mathbf{s}$ is the spin angular momentum, $\mathbf{l}$ is atomic orbital angular momentum, and $\mathbf{j}$ is the orbital angular momentum for envelope function. The total angular momentum of an exciton ($\mathbf{F}$) is the sum of the total angular momentum of hole ($\mathbf{J}_h$) and electron ($\mathbf{J}_e$) that make it up. See Ref. [53]
[56] Luo J W, Franceschetti A, Zunger A. Direct-bandgap InAs quantum-dots have long-range electron–hole exchange whereas indirect gap Si dots have short-range exchange. Nano Lett, 2009, 9, 2648
[57] Gupalov S V, Ivchenko E L. The fine structure of excitonic levels in CdSe nanocrystals. Phys Solid State, 2000, 42, 2030
[58] Krahne R, Morello G, Figuerola A, et al. Physical properties of elongated inorganic nanoparticles. Phys Rep, 2011, 501, 75
[59] Zhao Q Z, Graf P A, Jones W B, et al. Shape dependence of band-edge exciton fine structure in CdSe nanocrystals. Nano Lett, 2007, 7, 3274
[60] von Grünberg H H. Energy levels of CdSe quantum dots: Wurtzite versus zinc-blende structure. Phys Rev B, 1997, 55, 2293
[61] Ajiki H, Cho K. Fine structure of exciton in a quantum dot: Effect of electron–hole nonanalytic exchange interaction. Singapore: World Scientific, 2001, 77
[62] Gong K, Martin J E, Shea-Rohwer L E, et al. Radiative lifetimes of zincblende CdSe/CdS quantum dots. J Phys Chem C, 2015, 119, 2231
[63] Karel Čapek R, Moreels I, Lambert K, et al. Optical properties of zincblende cadmium selenide quantum dots. J Phys Chem C, 2010, 114, 6371
[64] Wang Q B, Seo D K. Synthesis of deep-red-emitting CdSe quantum dots and general non-inverse-square behavior of quantum confinement in CdSe quantum dots. Chem Mater, 2006, 18, 5764
[65] Deng Z T, Cao L, Tang F Q, et al. A new route to zinc-blende CdSe nanocrystals: Mechanism and synthesis. J Phys Chem B, 2005, 109, 16671
[66] Mohamed M B, Tonti D, Al-Salman A, et al. Synthesis of high quality zinc blende CdSe nanocrystals. J Phys Chem B, 2005, 109, 10533
[67] Alivisatos A P, Harris T D, Carroll P J, et al. Electron–vibration coupling in semiconductor clusters studied by resonance Raman spectroscopy. J Chem Phys, 1989, 90, 3463
[68] Hodes G, Albu-Yaron A, Decker F, et al. Three-dimensional quantum-size effect in chemically deposited cadmium selenide films. Phys Rev B, 1987, 36, 4215
[69] Allan G, Delerue C. Confinement effects in PbSe quantum wells and nanocrystals. Phys Rev B, 2004, 70, 245321
[70] Wang F D, Yu H, Jeong S, et al. The scaling of the effective band gaps in indium-arsenide quantum dots and wires. ACS Nano, 2008, 2, 1903
[71] Jasieniak J, Smith L, van Embden J, et al. re-examination of the size-dependent absorption properties of CdSe quantum dots. J Phys Chem C, 2009, 113, 19468
[72] Huxter V M, Kim J, Lo S S, et al. Spin relaxation in zinc blende and wurtzite CdSe quantum dots. Chem Phys Lett, 2010, 491, 187
[73] Kuno M, Nirmal M, Bawendi M G, et al. Magnetic circular dichroism study of CdSe quantum dots. J Chem Phys, 1998, 108, 4242
[74] Delerue C, Lannoo M. Nanostructures: Theory and modeling. Berlin, Heidelberg: Springer, 2013
[75] Takagahara T. Excitonic optical nonlinearity and exciton dynamics in semiconductor quantum dots. Phys Rev B, 1987, 36, 9293
[76] Kayanuma Y. Quantum-size effects of interacting electrons and holes in semiconductor microcrystals with spherical shape. Phys Rev B, 1988, 38, 9797
[77] Hilborn R C. Einstein coefficients, cross sections, *f* values, dipole moments, and all that. Am J Phys, 1982, 50, 982
[78] Liptay T J, Marshall L F, Rao P S, et al. Anomalous stokes shift in CdSe nanocrystals. Phys Rev B, 2007, 76, 155314

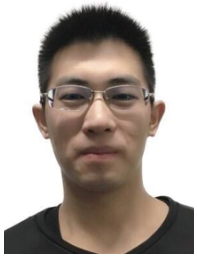

Zhimin Ji is a Ph.D. candidate in State Key Laboratory of Superlattices and Microstructures at Institute of Semiconductors CAS. His research focuses on the theoretical study of luminescence properties of semiconductor nanostructures, and the fabrication process of semiconductor lasers and optical amplifiers.

Zhigang Song Associate Researcher, graduated from the Institute of Semiconductors, Chinese Academy of Sciences (CAS) with a Ph.D. in 2017 and worked at the Max Planck Institute of Solid State Physics and Chemistry, Germany and Nanyang Technological University, Singapore, before returning to China to join the State Key Laboratory of Semiconductor Superlattices, Institute of Semiconductors, CAS in October 2020. He has been engaged in the simulation and design of semiconductor materials and devices.